Skeletal Radiol (2005) 34:19–28
DOI 10.1007/s00256-004-0848-9

SCIENTIFIC ARTICLE

A. Luna
S. Martinez
E. Bossen

Magnetic resonance imaging of intramuscular myxoma with histological comparison and a review of the literature

Received: 26 December 2003
Revised: 2 June 2004
Accepted: 27 July 2004
Published online: 22 October 2004

A. Luna (✉)
MR Unit, Clínica Las Nieves, Sercosa,
Carmelo Torres 2, 23007 Jaén, Spain
e-mail: aluna70@sercosa.com
Tel.: +34-953275601
Fax: +34-953275609

S. Martinez
Radiology Department,
Duke University Medical Center,
Durham, North Carolina, USA

E. Bossen
Pathology Department,
Duke University Medical Center,
Durham, North Carolina, USA

Abstract *Objective:* To evaluate the magnetic resonance (MR) features of intramuscular myxoma (IM) compared with its pathological findings. *Design:* Two radiologists retrospectively reviewed records and imaging studies of patients with histologically proven IM. Two radiologists also analyzed by consensus all the MR studies (pre- and post-contrast T1-weighted and T2-weighted sequences) and a pathologist reviewed the available histological material. *Patients:* Seventeen patients with 18 histologically proven IM were reviewed. Histological samples of 11 of these 18 tumors were available for pathological analysis. *Results:* There were 14 women and three men, with a mean age of 58.9 years. IM involved predominantly the thigh (n=10). MR imaging showed well-circumscribed intramuscular masses, hypointense on T1-weighted and hyperintense on T2-weighted images. Eleven masses were homogeneous and seven slightly heterogeneous due to fibrous septa. Enhanced MR imaging demonstrated three different patterns: peripheral enhancement (n=1), peripheral and patchy internal enhancement (n=7) or peripheral and linear internal enhancement (n=4). Intratumoral cysts were detected in four masses. MR imaging showed the presence of a pseudocapsule (n=12), fat around the lesion (n=16) and peritumoral edema (n=16). Histologically, all the tumors were hypocellular, hypovascular and myxoid. Peripheral areas of collagenous fibers formed a partial capsule and IM often merged into surrounding muscular fibers. More cellular tumors and those with scanty myxoid stroma tended to show a more prominent internal enhancement. *Conclusion:* IM shows several recognizable MR features which suggest its diagnosis.

Key words Magnetic resonance (MR) · Intramuscular myxoma · Soft tissues, neoplasms · Soft tissues, MR

Introduction

Intramuscular myxoma (IM) is a benign intramuscular neoplasm composed of fibroblasts and abundant myxoid stroma. Since its description by Stout [1] in 1948, its pathological features have been well studied. Although its definitive diagnosis depends on its histological analysis, imaging studies constitute the first step in its evaluation. Because of its low incidence, there are limited reports showing non-specific imaging characteristics. The plain film can be normal, show a soft tissue mass or, rarely, show calcifications within it [2, 3, 4]. Due to its hypovascular nature, IM shows a mild uptake on scintigraphic studies [4] and either poor or moderate vascularity on angiography [4, 5], although a moderate vascularity has been related to an increase in the cellularity [4]. A well-demarcated hypoechoic or anechoic mass with multiple cystic areas or fluid-filled clefts in an intramuscular location is the typical presentation on ultrasound studies [6, 7, 8]. On computed tomography (CT), IM is shown as a

well-defined, homogeneous mass with attenuation values between those of water and muscle [4, 5, 8, 9].

The MR features have been reported in less than 123 cases [7, 8, 9, 10, 11, 12, 13, 14, 15, 16, 17, 18, 19, 20, 21, 22, 23, 24, 25, 26, 27, 28, 29, 30, 31, 32, 33, 34, 35, 36, 37, 38, 39, 40, 41] and a few of these studies were performed with intravenous contrast material [8, 10, 13, 14, 15, 15, 17, 36, 37, 38, 39, 40, 41]. Peterson et al. [10] established distinguishing MR criteria for its diagnosis and Bancroft et al. [37] and Murphey et al. [38] have added new data recently.

This study presents the radiological characteristics of this tumor, focusing on the MR and pathological findings in an attempt to further characterize its most common appearance and possible atypical presentations.

Materials and methods

A retrospective evaluation of 17 patients with 18 histologically proven IM studied by MR imaging was performed. None of the cases included in this series has been previously reported. Our study included 14 women and three men, with ages ranging from 39 to 75 years (mean 58.9 years). Fifteen cases were identified using the database of the Pathology Department of two different institutions, and the remaining two from the consultation files of another institution. The diagnoses were based on the pathological report of the resected tumor in all cases. A review of the available charts, MR studies and histological materials was carried out. Due to the retrospective nature of this study, the review of the pathological material could be performed in only 11 cases, because no samples from the specimens were available in the rest of the cases.

Imaging analysis

MR sequences varied because they were obtained in different institutions, but in all cases conventional spin-echo (SE) T1-weighted (TR: 450–600, TE: 10–20) and SE and fast spin-echo (FSE) T2-weighted (TR: 2300–2900, TE: 80–120) sequences were performed. Additional sequences included Short-Tau Inversion Recovery (STIR) (TR: 2000–4200, TE: 15–20, TI: 140–160) and T2-weighted gradient-echo (GE) (TR: 400–600, TE: 12–15, flip angle: 30°). All MR studies except for one (case 8) included either a STIR (n=6) or a fat-saturated FSE T2-weighted image (n=10). All the patients were studied in a 1.5 T magnet, except for one (1.0 T magnet). Intravenous gadopentetate dimeglumide of gadolinium (GDG) was used in 12 patients. Fat suppression was used in the post-contrast images in eight cases.

Two radiologists reviewed the MR examinations, with agreement by common consensus. The masses were analyzed taking into account the following features: anatomical location, size, margins, homogeneity, presence of capsule, peritumoral edema, presence of fat either intralesionally or surrounding the lesion, signal intensity characteristics on T1-weighted, T2-weighted and post-contrast images (12 of 18 masses), and presence of cysts. The size was determined using the largest diameter of the tumor. The margins were defined as sharp when more than 90% of the tumor rim was sharply demarcated from the surrounding tissues, as lobulated when the tumor was sharply demarcated but presenting some bulges in its contour and as ill-defined when more than 75% of the margin was unsharp. The homogeneity was evaluated on T2-weighted images, considering the mass as homogeneous when the whole lesion had the same signal intensity, or slightly heterogeneous when predominant background signal intensity was identified with linear stranding in its interior like fibrous septa. When a feathery zone of high signal intensity was seen extending from the margins of the tumor to the surrounding tissues on T2-weighted sequences, it was called edema. The edema was more conspicuous on STIR or fat-saturated FSE T2-weighted sequences. A capsule-like structure was considered when a rim of low signal intensity at the tumor periphery was demarcated by adjacent muscular edema on T2-weighted sequences. Identification of fat adjacent to the lesion at any point was considered as peritumoral fat. The presence of intratumoral fat was also evaluated. Three patterns of enhancement were defined after the use of GDG: (1) peripheral enhancement of the mass without any internal enhancement (Fig. 1); (2) peripheral and internal enhancement with linear stranding inside the tumor (Fig. 2); and (3) peripheral enhancement and central areas with focal patchy enhancement (Fig. 3). The presence of intratumoral cysts, defined as focal round areas without internal contrast uptake

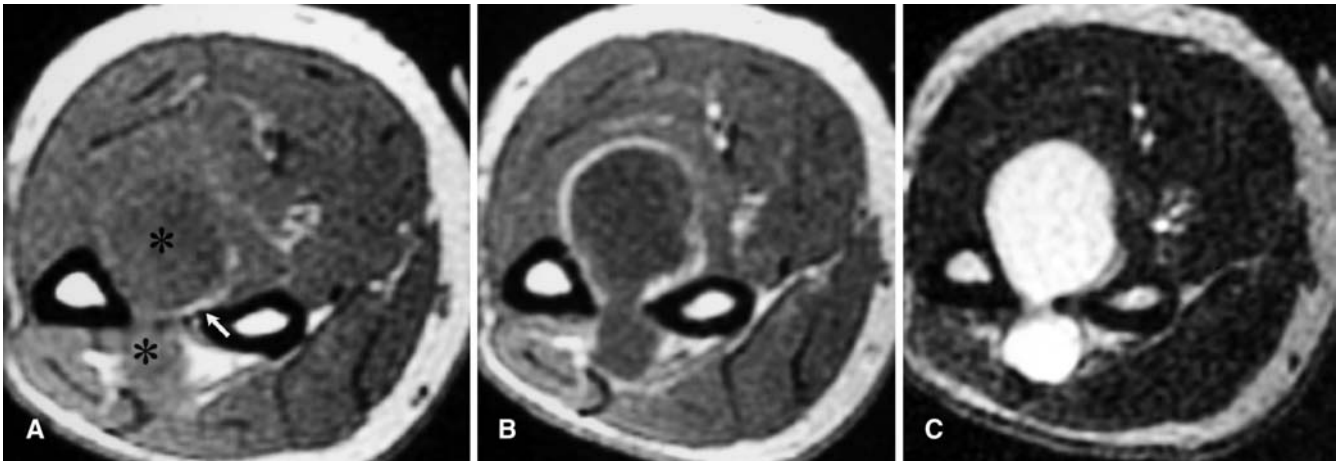

Fig. 1A—C Case 9. Intramuscular myxoma in a 71-year-old caucasian man. **A** Transverse T1-weighted spin-echo MR image shows a bilobular homogeneous low-signal-intensity mass in the interval brachioradialis and flexor carpi muscles (*asterisks*). Fat around the lesion is identified (*white arrow*). **B** After the administration of gadolinium there is a marked peripheral uptake without any sign of internal enhancement (type 1pattern). **C** Axial FSE T2-weighted MR image shows a homogeneous mass with a high signal intensity similar to that of fluid

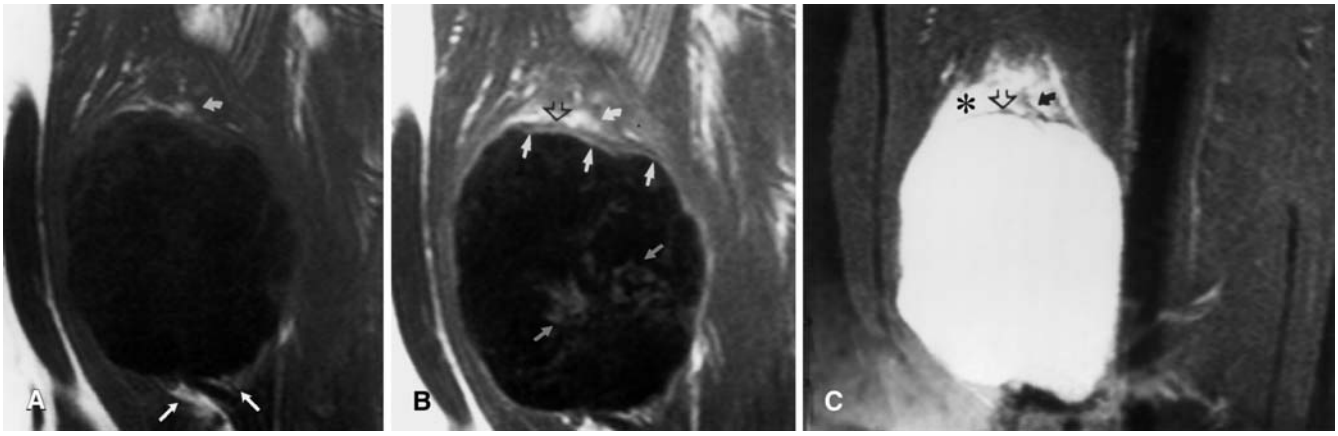

Fig. 2A—C Case 13. Intramuscular myxoma in a 48-year-old caucasian woman. **A** Coronal T1-weighted MR image shows a lobulated hypointense mass mildly heterogeneous in its interior with peripheral fat in the superior (*curved arrow*) and inferior (*straight arrows*) poles in the abductor magnus muscle. **B** Coronal T1-weighted MR image after the administration of gadolinium demonstrates peripheral (*straight white arrows*) and subtle linear internal enhancement (*gray arrows*) (type 2 pattern). Peritumoral fat (*curved arrow*) and a hypointense line (*open arrow*) consistent with the pseudocapsule are seen. **C** Coronal fat-suppressed FSE T2-weighted MR image shows the presence of edema (*asterisk*) in the muscles surrounding the superior pole of the mass with an adjacent area of low signal representing suppressed fat (*curved arrow*) (it was hyperintense in **A**) and a hypointense peripheral line representing the pseudocapsule (*open arrow*)

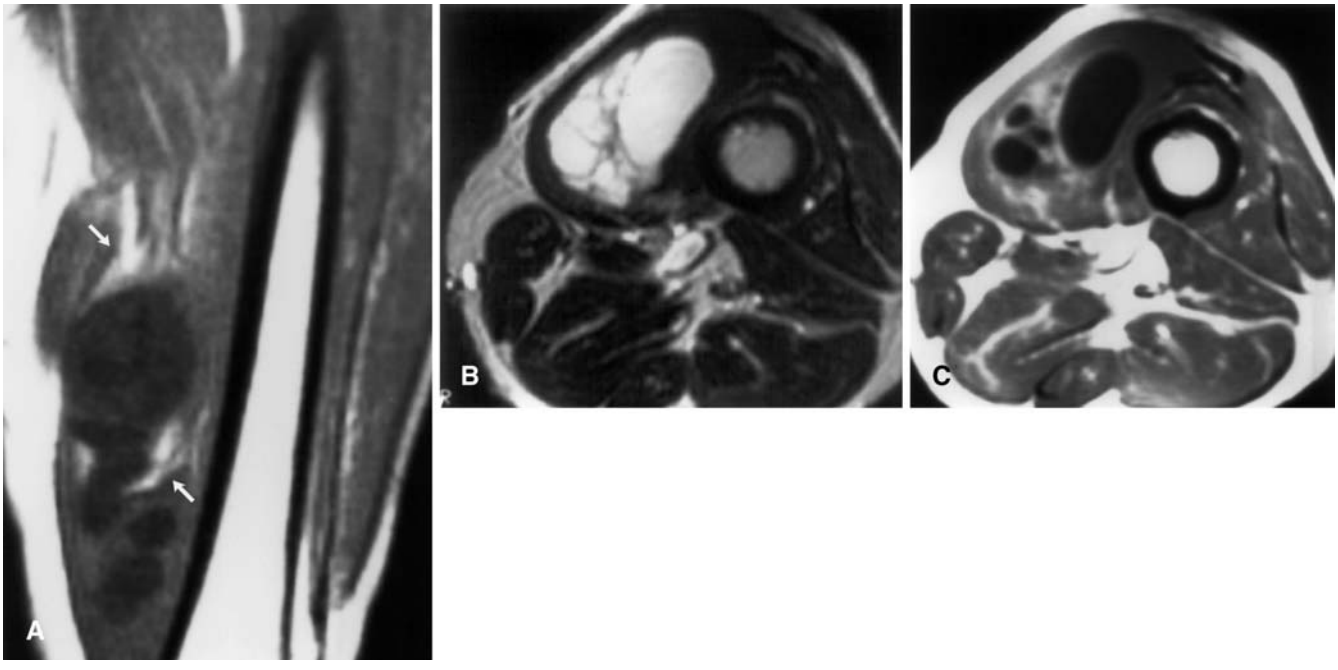

Fig. 3A—C Case 4. Intramuscular myxoma in a 66-year-old caucasian woman. **A** Sagittal T1-weighted spin-echo MR image shows a multiloculated low-signal-intensity and mildly heterogeneous mass located in the right vastus medialis, surrounded by fat (*white arrows*). **B** Axial FSE T2-weighted MR image demonstrates two different components, one homogeneous and other mildly heterogeneous, due to a prominent internal linear stranding. Both components show high signal intensity, similar to that of fluid. **C** Axial post-contrast T1-weighted MR image at the same level demonstrates areas with marked patchy internal enhancement, corresponding to an IM with type 3 pattern. Notice the presence of cystic areas within the tumor

but with thin peripheral enhancement (Fig. 3), was also analyzed. These cystic areas also demonstrated low signal intensity on T1-weighted-images and markedly high signal intensity on T2-weighted images.

Pathological analysis

A musculoskeletal pathologist with more than 20 years of experience reviewed the available specimens of 11 tumors (cases 6 to 16 of Table 1 and Table 2). Multiple sections of each specimen including sections of the whole tumor were made except for three

Table 1 Clinical data (*U* unknown, *C* caucasian, *AA* Afro-American, *NA* not available, *NR* no recurrence, *FD* association with fibrous dysplasia, *FNA* fine needle aspiration, *ML* myxoid liposarcoma, *NSMT* non-specific myxoid tumor, *IM* intramuscular myxoma, *MS* myxoid sarcoma)

Patient no.	Age (years)	Sex	Race	Location	Size (cm)[a]	Symptoms/Time[b]	Follow-up (months)	FD	FNA
1[c]	54	M	U	Deltoid	7×7×5 3×3×2	Mass/18	NA	Yes	No
2	58	F	U	Vastus medialis	5×3×2	NA	NA		No
3	66	F	C	Rectus femoris	4×3×3	Mass/36	Recurrence	Yes	No
4	66	F	C	Vastus medialis	9×4×4	Mass/60	NR 30		No
5	75	F	C	Gluteus maximus	6×5×7	Mass/48	NR 6		ML
6	64	F	C	Rectus femoris	2×6×4	Mass/1	NA		NSMT
7	41	F	C	Adductor maximus	6×3×3	Mass/24	NR 60		No
8	57	M	AA	Lattissimus dorsi	9×8×9	Incidental on CT	NR 120		NSMT
9	71	F	C	Forearm[d]	5×3×3	Mass/10[d]	NR 3		No
10	39	F	C	Vastus lateralis	2×2×2	Mass/12	NA		No
11	52	M	C	Triceps	4×2×3	Mass/14	NR 48		IM
12	49	F	C	Deltoid	5×4×4	Mass/72	NR 16		ML
13	48	F	C	Abductor magnus	7×6×5	Mass/8	NR 4		MS
14	72	F	C	Vastus intermedius	7×3×3	Mass/72	NR 3		NM
15	62	F	AA	Vastus medialis	3×4×3	Mass/6	NR 1		NSMT
16	65	F	C	Longissimus thoracis	3×2×3	Pain/6	NA		NSMT
17	63	F	C	Gastrocnemius	9×6×4	Mass/84	NR 12		No

[a] Size in centimeters in craniocaudal, transverse and anteroposterior diameters respectively
[b] Clinical form of presentation/time of evolution in months
[c] Case 1 presented two deltoid masses
[d] In case 9 the tumor was localized between brachiradialis and flexor carpi, through the interosseous membrane

Table 2 MR findings (*H* homogeneous, *S Het* slightly heterogeneous, *T1* signal intensity on T1-weighted images, *Hypo* hypointense, *T2* signal intensity on T2-weighted images, *Hyper* hyperintense, *GDG* pattern of enhancement after administration of gadopentetate diglumide and presence or absence of cysts, *1* peripheral enhancement without internal enhancement, *2* peripheral and linear internal enhancement, *3* peripheral and patchy internal enhancement, *C* presence of cysts)

Patient no.	Margins	Homogeneity	T1	T2	GDG	Capsule	Edema	Fat
1	Lobulated	H	Hypo	Hyper	No	No	Yes	Yes
	Lobulated	H	Hypo	Hyper	No	No	Yes	Yes
				Hyper	No	No	Yes	Yes
2	Sharp	H	Hypo	Hyper	No	No	Yes	Yes
3	Sharp	H	Hypo	Hyper	2	Yes	Yes	Yes
4	Lobulated	S Het	Hypo	Hyper	3/C	Yes	Yes	Yes
5	Lobulated	S Het	Hypo	Hyper	2	Yes	Yes	Yes
6	Lobulated	S Het	Hypo	Hyper	No	No	Yes[a]	Yes
7	Sharp	H	Hypo	Hyper	No	Yes	Yes	Yes
8	Sharp	S Het	Hypo	Hyper	No	No	NA[b]	Yes
9	Lobulated	H	Hypo	Hyper	1	Yes	Yes	Yes
10	Sharp	H	Hypo	Hyper	3	No	Yes	No
11	Lobulated	S Het	Hypo	Hyper	2	Yes	Yes	Yes
12	Sharp	H	Hypo	Hyper	2	Yes	Yes	Yes
13	Lobulated	S Het	Hypo	Hyper	3	Yes	Yes	Yes
14	Sharp	H	Hypo	Hyper	3	Yes	Yes	Yes
15	Sharp	H	Hypo	Hyper	3/C	Yes	Yes	No
16	Lobulated	H	Hypo	Hyper	3/C	Yes	Yes	Yes
17	Lobulated	S Het	Hypo	Hyper	3/C	Yes	Yes	Yes

[a] In case 6 a fine needle aspiration (FNA) was performed 15 days before MR, imaging; therefore, the presence of edema was not considered in the final analysis
[b] In case 8 the presence of edema was not assessable because the only T2-weighted sequence available was a gradient-echo

cases in which the periphery of the lesion was not available. All sections were embedded in paraffin and stained with hematoxylin-eosin. An estimation of cellularity was made by counting non-vascular nuclei in three random high-power fields (×40) and obtaining an average number of nuclei per high-power field. The results were divided into three categories: 1+, <40 nuclei per high-power field; 2+, 40–60 nuclei per high-power field; 3+, >60 nuclei per high-power field. As the cellularity grade varied within the same tumor, each mass was classified according to the overall grade of cellularity. Fibrous bands were classified from 0 to 3+ according to their prominence in microscopic sections. Pseudocysts, defined as spaces without an epithelial lining, were divided into micropseudocysts (<2 mm diameter) and macropseudocysts (>2 mm diameter). Because the analysis was retrospective, direct

correlation of MR findings of individual tumors was limited, since specific sample areas were not known at the time of the surgical pathology examination.

Results

Clinical results

Table 1 lists the clinical and pathological data of the patients in the study. The tumors involved the thigh muscles (n=10), the upper arm and shoulder (n=4) and the forearm, gluteus, paraspinal and chest wall muscles one each. The tumor diameter measured by MR imaging varied from 2.5 to 9 cm (mean average 5.7 cm) at the moment of the diagnosis. The predominant form of presentation was a painless mass in 14 of 16 patients (88%); this information was not available in one patient. The clinical symptoms lasted from 1 month to 7 years. There were two cases of Mazabraud's syndrome (Fig. 4). Post-surgical follow-up was available in 12 patients (mean time 29.7 months, range 1–84 months). There was only one recurrence in a case of Mazabraud's syndrome.

Nine patients underwent a fine needle aspiration (FNA) prior to surgery. A diagnosis of IM was established in one case; the rest of the results of the FNA are listed in Table 1. In all patients the histological diagnosis of IM was established according to the pathological report of the excised tumor.

MR findings

Table 2 summarizes the MR findings. All 18 masses showed the bulk of the tumor with predominantly high signal intensity on T2-weighted images, and all were clearly hypointense on T1-weighted images. Eleven masses were completely homogeneous (Figs. 1, 4), and the remaining seven were slightly heterogeneous (Figs. 2, 3), probably due to the presence of fibrous septa. Ten tumors showed discrete lobulations (Fig. 4), although eight were sharply demarcated (Figs. 1, 2, 3). None of the tumors presented ill-defined borders. Edema in the surrounding muscles was identified in all masses (Fig. 2) in cases where T2-weighted or STIR images were available (this includes 17 masses in our series). Fat surrounded the lesion in 16 masses (Figs. 1, 2, 3), always showing a predilection for the superior and inferior poles of the lesion, although two tumors were entirely surrounded by fat. Edema was more commonly observed around both poles of the IM. Five masses also presented edema around the equator of the lesion. A capsule was identified in 12 masses on T2-weighted sequences (Fig. 2). Following the intravenous administration of GDG, seven patients had type 3 enhancement (Fig. 3), four tumors type 2 (Fig. 2) and one tumor had negligible internal enhancement of type 1 (Fig. 1). Cysts were identified in four masses (Fig. 3), all of them in tumors with type 3 enhancement patterns.

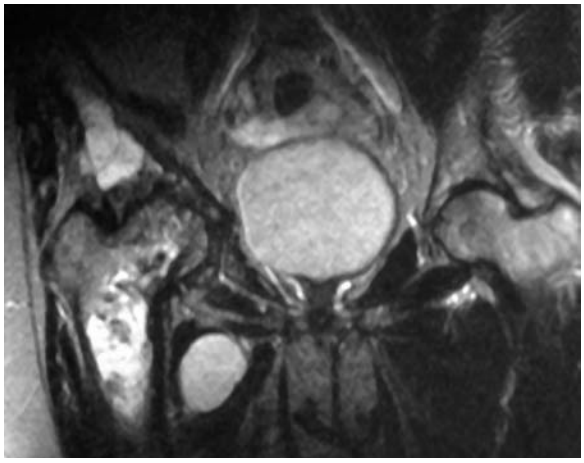

Fig. 4 Case 3. Mazabraud's syndrome in a 66-year-old caucasian woman. Coronal FSE T2-weighted MR image demonstrates typical changes of fibrous dysplasia in right pelvis and femur, with the presence of an IM in the medial thigh

Pathological findings

Macroscopically, the myxomas were described as gelatinous masses. Neither hemorrhage nor necrosis was identified. Microscopic examination showed the bulk of the neoplasm to consist of paucicellular myxoid tissue with sparse blood vessels associated with fibrous bands. None of these tumors presented areas of significantly increased vascularity. The lower the cellularity the more abundant the myxoid component of the tumor tended to be (Fig. 5A). The results are tabulated in Table 3, which shows three of the tumors to have 1+ cellularity, 3 to have 2+ cellularity, and 5 to have 3+ cellularity.

In all cases with available sections of the periphery of the lesion (n=8), myxomas extended into adjacent muscle, dividing the muscle into small groups of fibers, some of them atrophic. Empty spaces separating muscular fibers were consistent with edema (n=8) (Fig. 5B). In addition to muscular infiltration, there was a condensation of fibrous tissue no more than 1–2 mm in thickness and discontinuous at the myxoma/muscle junction, producing a distinct partial fibrous capsule in seven of the eight specimens with sections of the myxoma/muscle junction (Fig. 5B, C). Although fat cells were identified around the lesion in all cases, no extensive samples of the periphery of the tumor were available.

Internal fibrous bands were also present within most of the tumors (Table 3, Fig. 5D). Cyst-like areas were identified in one case at the time of the gross examination (case 8). Microscopically, pseudocysts were identified in

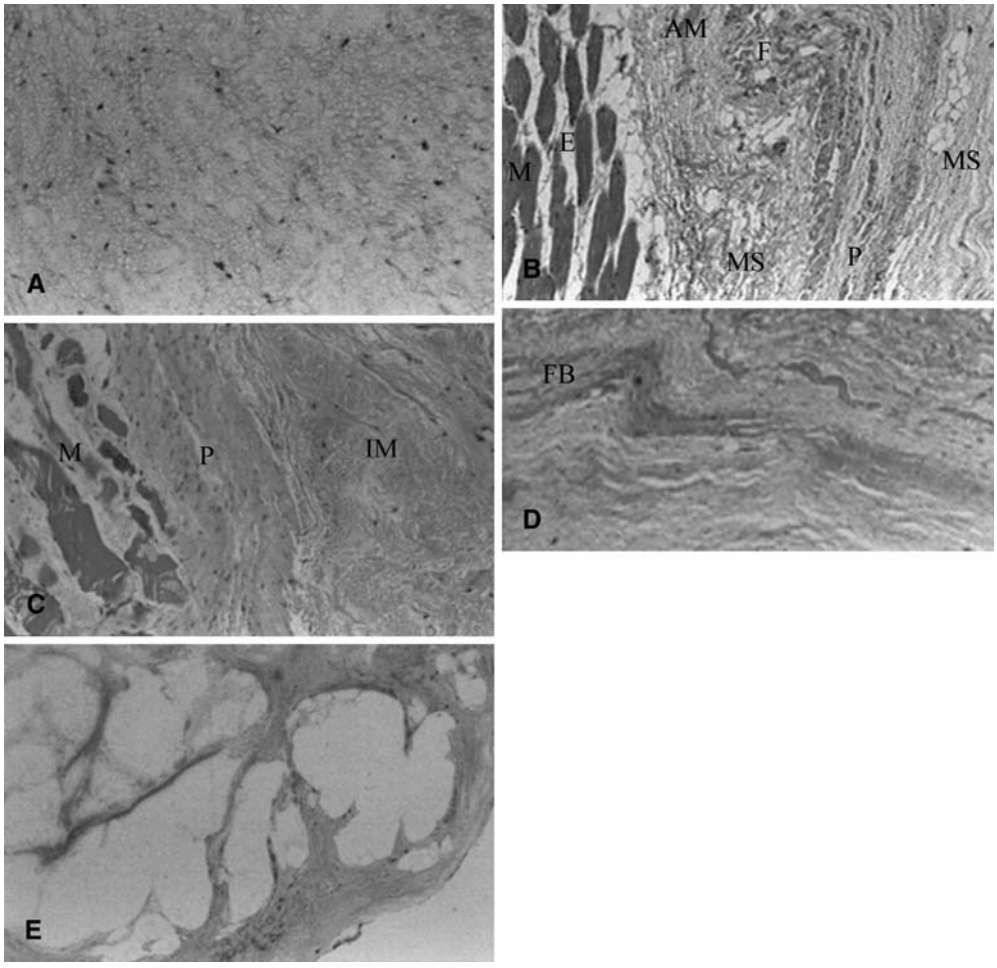

Fig. 5A—E Microscopic pathological findings of intramuscular myxoma. (**A**) Specimen from case12 (hematoxylin-eosin stain; original magnification ×13.2) shows the typical appearance of a basic myxomatous area, composed of scarce round or spindle cells enmeshed within an abundant myxoid stroma with rare blood vessels. **B** Specimen from case 12 (hematoxylin and eosin stain; original magnification ×13.2) demonstrates normal muscle (*M*) fibers separated by empty spaces representing edema (*E*). Atrophic muscles (*AM*) and fat cells (*F*) are also demonstrated. In this section the pseudocapsule (*P*) is separating myxomatous stroma (*MS*). **C** Specimen from case 15 (hematoxylin-eosin stain; original magnification ×13.2) shows a peripheral condensation of fibrous tissue, representing the pseudocapsule (*P*), separating normal muscle (*M*) from myxoid tissue (*IM*). **D** Specimen from case 12 (hematoxylin-eosin stain; original magnification ×13.2) shows a fibrous band (*FB*) within myxoid tissue. **E** Specimen from case 10 (hematoxylin-eosin stain; original magnification ×3.3) demonstrates multiple spaces without epithelial lining representing macropseudocysts

six masses (Table 3, Fig. 5E). Four of the 11 tumors had micropseudocysts and two, macropseudocysts. Case 8, which was reported as containing a cyst in the gross examination, had only microcysts microscopically. The explanation for this could be either that no attempt was made to sample the gross cyst or that the cyst was too large to be demonstrated on a slide.

MR-pathological correlation

In the 11 patients with available pathology specimens, a correlation between the MR and pathological findings was carried out for the presence of fibrous septa and the presence of a capsule, with the help of T2-weighted images and the cellularity and presence of pseudocysts with the enhancement pattern.

Of the 11 cases, seven had a homogeneous appearance on T2-weighted images, six of which (86%) showed scarce fibrous bands (groups 0, 1+) on the microscopic analysis, and four masses had slightly heterogeneous appearance, three of which (75%) showed abundant fibrous bands (groups 2+, 3+).

The periphery of the myxoma was only partially sampled in eight masses. Six had segments of a capsule on T2-weighted images and partial capsule on the microscopic analysis, showing a strong radio-pathological correlation, while two had no capsule on MR but a partial

Table 3 Microscopic pathological findings and enhancement patterns

Patient no.	Cellularity[a]	Fibrous bands[b]	Partial capsule	Pseudocysts[c]	GDG[d]
6	3+	1+	Yes	No	No
7	2+	3+	Yes	No	No
8	3+	3+	Not sampled	Micro	No
9	1+	1+	Not sampled	No	1
10	2+	1+	Muscle only	Macro	3
11	1+	3+	Yes	Macro	2
12	1+	1+	Yes	Micro	2
13	3+	2+	Not sampled	Micro	3
14	3+	1+	Yes	No	3
15	2+	1+	Yes	Micro	3/C
16	3+	0	Yes	No	3/C

[a] Cellularity determined by nuclei per ×40 objective field: 1+, <40; 2+, 40–60; 3+, >60
[b] Fibrous, classified into 1+ to 3+, estimates the prominence of fibrous bands in microscopic sections
[c] Pseudocysts are classified as microcysts <2 mm in maximum diameter or macrocysts >2 mm in maximum diameter
[d] Pattern of enhancement after administration of gadopentetate diglumide and the presence or absence of cysts. *1*, peripheral enhancement without internal enhancement; *2*, peripheral and linear internal enhancement; *3*, peripheral and patchy internal enhancement; *C*, presence of cysts

capsule was identified pathologically in one. The absence of fat in the periphery of these eight masses may be due to the lack of good sampling of the upper and inferior poles.

All eight tumors with enhanced MR studies and pathological analysis showed peripheral enhancement, with seven showing mild internal enhancement and one with a complete absence of internal enhancement. All tumors with a higher level of cellularity showed patchy internal enhancement (n=5), with two also showing internal cystic areas on MR imaging. Three tumors had poor cellularity and were rich in myxoid stroma, of which one had absence of enhancement and two had linear internal enhancement; this lineal enhancement represented fibrous bands. Therefore, the presence of more prominent enhancement in this series is related to tumors with more cells and less myxoid tissue. The histological presence or absence of pseudocysts and their size did not seem to influence the presence or absence of internal enhancement.

Discussion

Clinical, demographic and location data in our series correlated well with those observed in other studies, except for our larger female/male ratio (3:1). Pathological findings in our series are similar to the classic histological description of IM. Our data are also consistent with previous literature [39] rendering a specific diagnosis of IM with FNA in only 1 of 9 cases. This is due to the scant cellularity and the non-specific cytological features of IM [12]. Moreover, as in this series, areas of increased cellularity have been previously reported, which raises the likelihood of making an erroneous diagnosis of myxoid sarcoma [42]. Therefore, a surgical biopsy is necessary for definitive diagnosis.

The MR appearances of this tumor have recently been shown to be more diverse [37, 38] than previously described [10], with complete or partial capsule, intratumoral cysts, surrounding fat rim or cap and surrounding muscular edema being added to its typical cystic appearance.

On T2-weighted images, seven masses presented a heterogeneous appearance in our series, due to the presence of a fine linear stranding within the tumor, representing thin fibrous septa. This finding has been reported previously in the literature [12, 37, 38], and in previous ultrasound descriptions [8]. Moreover, microscopic analysis in our series demonstrated scarce fibrous bands in 86% of the cases with a homogeneous appearance, and more prominent and numerous fibrous bands in 75% of the tumors with linear stranding on MR imaging.

Most of the previously reported cases [8, 10, 13, 14, 15, 16, 17, 18, 33, 36, 37, 38, 40, 41] evaluated by GDG had either heterogeneous internal enhancement or peripheral enhancement with occasional fine internal septa. All 12 tumors analyzed with post-contrast sequences in our series showed peripheral enhancement which corresponded to the described pseudocapsule of the pathological literature [39, 43]. Microscopically, the junction of the tumor with the adjacent tissue did not form a well-defined capsule, but there were areas of condensation of collagen fibers forming a partial capsule in seven out the eight cases where samples of the periphery of the tumors were available for pathological analysis. On T2-weighted images, this pseudocapsule corresponded to a hypointense rim surrounding the periphery of the tumor, and was identified on six of the seven masses with confirmed partial capsule on the histological analysis while not being present in the only mass that did not show this feature histologically.

In our limited histological analysis, all five masses with patchy internal enhancement had rich cellularity and scant myxoid matrix whereas tumors without internal enhancement (*n*=1) or with internal linear stranding representing fibrous septa (*n*=2) had poor cellularity and abundant myxoid matrix. Therefore, tumors with rich cellularity and less myxoid matrix showed more prominent internal enhancement in this series. No focal areas of increased vascularization were identified in any mass. Unlike our findings, recently reported data described the enhancement as proportional to the amount of myxoid tissue [36] or related to focal areas of relative hypervascularity [37].

Cysts were demonstrated within four masses in post-contrast images in this series (33%). In contrast to the recent literature [38], we did not find agreement between the identification of cysts on MR imaging and pathological examination and there was no relationship between either the presence or number of pseudocysts and the different enhancement patterns.

The presence of edema has been related to IM in the pathological and, recently, the radiological literature [37, 38, 41]. Every mass with a SE or FSE T2-weighted sequence in our series showed this feature, more commonly around both poles of the lesion, although it was surrounding the equatorial zone of the tumor in five cases. The presence of edema sometimes involved a slight loss of sharpness in the poles, but it also allowed the indirect visualization of a pseudocapsule in 75% of the masses. The edema corresponded pathologically to portions of the tumor merged with the adjacent muscle, separating the fibers and creating empty spaces. Edema has also been related either to the extension of mucoid material from the tumor into adjacent muscle fibers [38] or to secondary irritation of the muscular tissue [41].

Another frequent finding on MR imaging in this series was the presence of fat around both poles in 89% of the lesions, which has been reported previously [7, 37, 38, 41], and has been related pathologically to fatty muscle atrophy [38] due to the infiltrative pattern of slow growth of IM [37]. However, microscopic analysis of our cases has not revealed the presence of significant fat around the lesion, probably due to the absence of extensive samples of the periphery of the tumors. In two cases, a more prominent fat deposit around almost the whole mass was observed on MR imaging, which may be secondary to displacement of intra- and intermuscular fatty connective tissue by the tumor, as reported in the previous pathological literature [12].

The association between IM and fibrous dysplasia is known as Mazabraud's syndrome. Sixty cases [13, 17, 18, 25, 26, 27, 32, 33, 35, 36, 38, 44, 45, 46, 47, 48, 49, 50, 51, 52, 53, 54, 55, 56, 57, 58, 59, 60, 61, 62, 63] have been described in the literature, including the two cases of the present series. IM when associated with fibrous dysplasia presents some distinctive features: (1) it is usually in the vicinity of the bone with a more extensive area affected; (2) multiplicity of the IM is common; (3) local recurrence of IM after surgery has been reported in six cases [26, 42, 50]. One IM associated with Mazabraud's syndrome in this series demonstrated multiplicity and the other recurrence after excision. The MR appearance of IM associated with fibrous dysplasia shows no differences from the solitary form of IM in the 17 reported cases in the literature [13, 17, 18, 25, 26, 27, 32, 33, 35, 36, 38], as in this series.

Cystic masses such as synovial cysts, ganglions, lymphoceles or seromas may mimic the appearance of IM on unenhanced MR imaging, but an intramuscular location of these conditions is uncommon and they are usually truly cystic, non-enhancing lesions [38]. IM must also be differentiated from deep myxoid lesions localized in the extremities. This group includes [64]: myxoid peripheral nerve sheath tumors, extraskeletal myxoid chondrosarcoma, myxoid liposarcoma, myxofibrosarcoma, myxoid leiomyosarcoma, low-grade fibromyxoid sarcoma (LGFMS) and cellular myxoma (CM).

Benign and 10% of malignant peripheral nerve sheath tumors [64] may have a large myxoid component. Most of the time, they are intermuscular and related to a nerve [38]. The most important imaging feature for their recognition is their typical fusiform morphology, which represents the tubular entering and exiting nerve [65]. On MR imaging, extraskeletal myxoid chondrosarcoma, like IM, appears as brighter than muscle on T2-weighted images [11, 12, 13], with mild peripheral to septal enhancement after contrast material injection [66]. However, unlike IM, it appears as a heterogeneous ill-defined mass with variable signal intensity on T1-weighted images [11, 12, 13]. The presence of areas of chondroid matrix mineralization can also allow their differentiation [66]. Myxoid liposarcoma is the most common source of confusion with IM when the myxoid component is high [7, 64]. It is usually a well-defined and septated mass, hypointense [67, 68] or isointense [69] to muscle on T1-weighted images and hyperintense on T2-weighted images. Features that distinguish it from IM are its commonly intermuscular location [38], the presence of internal lacy and linear foci of high signal on T1-weighted images representing fat [67, 70], and a heterogeneous and more diffuse enhancement after GDG administration than the typical patterns of IM [71]. Myxofibrosarcoma is a subtype of malignant fibrous histiocytoma, more heterogeneous and ill-defined than IM [72], but like IM it also is very hyperintense on T2-weighted images and typically shows peripheral nodular enhancement [11, 73]. To our knowledge there are no reported MR imaging descriptions of LGFMS, CM and myxoid leiomyosarcoma. LGFMS and CM are two recently reported benign myxoid tumors with the potential for recurrence, clinically similar to IM [64].

In clinical practice, MR imaging findings raise the suspicion of IM in cases of an intramuscular mass with a cystic appearance on unenhanced sequences, with pe-

ripheral and a variable degree of internal enhancement on post-contrast images, and possibly the identification of intratumoral cystic areas. The most distinctive features of IM are the identification of a perilesional fat ring and the presence of edema in adjacent muscles [37].

Inherent limitations of our study are related to the small number of cases included. Because of its retrospective character and its multi-institutional origin, it was not possible to have a standard MR protocol or a direct correlation between the MR and pathological findings.

In conclusion, IM must be suspected in a patient over 40 years, often a woman, presenting with a painless mass involving a proximal large group of muscles (usually the anterior thigh). Radiologically, the tumor is intramuscular with usually a cystic-like appearance, mostly homogeneous on conventional MR imaging. The presence of fat or edema in the surrounding muscles is frequent. The use of GDG can help in its characterization as this tumor most commonly shows peripheral and internal enhancement. Other features of IM are the presence of internal cystic areas.

References

1. Stout AP. Myxoma, the tumor of primitive mesenchyme. Ann Surg 1948; 127:706.
2. Ireland DCR, Soule EM, Ivins JC. Myxoma of the somatic soft tissue. Mayo Clin Proc 1973; 48:401.
3. Kindblom KL, Stener B, Angerball L. Intramuscular myxoma. Cancer 1974; 34:1737–1744.
4. McCook TA, Martinez S, Korobkin M, et al. Intramuscular myxoma. Radiographic and computed tomographic findings with pathologic correlation. Skeletal Radiol 1981; 7:15–19.
5. Ekelund L, Herrlin K, Rydholm A. Computed tomography of intramuscular myxoma. Skeletal Radiol 1982; 9:14–16.
6. Petterson H, Hudson TM, Springfield DS, Kaude JV. Cystic intramuscular myxoma. Acta Radiol Diagn 1985; 26:425–426.
7. Kransdorf MJ, Moser RP, Jelinek JS, Weiss SW, Benton PC, Berry BH. Intramuscular myxoma: MR features. J Comput Assist Tomogr 1989; 13:836–839.
8. Fornage BD, Romsdahl MM. Intramuscular myxoma: sonographic appearance and sonographically guided needle biopsy. J Ultrasound Med 1994; 13:91–94.
9. Kransdorf MJ, Murphey MD. Tumors of uncertain origin. In: Imaging of soft tissue tumors. Philadelphia: WB Saunders, 1997:353–357.
10. Peterson KK, Renfrew DL, Feddersen RM, Buckwalter JA, El-Khoury GY. Magnetic resonance imaging of myxoid containing tumors. Skeletal Radiol 1991:20:245–250.
11. Abdelwahad IF, Kenan S, Hermann G, Lewis MM, Klein MJ. Intramuscular myxoma: magnetic resonance features. Br J Radiol 1992; 65:485–490.
12. Caraway NP, Staerkel GA, Fanning CV, Varma DG, Pollock RE. Diagnosing intramuscular myxoma by fine-needle aspiration. Diagn Cytopathol 1994; 11:255–261.
13. Aoki T, Koulo H, Hisaoka M, Hashimoto H, Nakata H, Sakai A. Intramuscular myxoma with fibrous dysplasia: a report of two cases with review of the literature. Pathol Int 1995; 45:165–171.
14. Ma LD, Frassica FJ, McCarthy EF, Bluemke DA, Zerhouni EA. Benign and malignant musculoskeletal masses: MR imaging differentiation with rim-to-center differential enhancement ratios. Radiology 1997; 202:739–744.
15. Schwartz HS, Walker R. Recognizable magnetic resonance imaging characteristics of intramuscular myxoma. Orthopedics 1997; 20: 431–435.
16. May DA, Good RB, Smith DK, Parsons TW. MR imaging of musculoskeletal tumors and tumor mimickers with intravenous gadolinium: experience with 242 patients. Skeletal Radiol 1997; 26:2–15.
17. Court-Payen M, Jensen LI, Bjerregaard B, Schwarz G, Skjoldbyi B. Intramuscular myxoma and fibrous dysplasia of bone: Mazabraud's syndrome. Acta Radiol 1997; 38:368–371.
18. Kransdorf MJ, Murphey MD. Case of the month: Mazabraud's syndrome. Radiology 1999; 212:129–132.
19. Kilcoyne RF, Richardson MJ, Porter BA, Olson DO, Greenlee TK, Lanzer W. Magnetic resonance imaging of soft-tissue masses. Clin Orthop 1988; 228:13–18.
20. Totty WG, Murphy WA, Lee JKT. Soft-tissue tumors: MR imaging. Radiology 1986; 160:135–141.
21. Moulton JS, Biebea JS, Dunco DM, Braley SE, Bisset III GS, Emery KH. MR Imaging of soft-tissue masses: diagnostic efficacy and value of distinguishing between benign and malignant lesions. AJR Am J Roentgenol 1995; 164:1191–1199.
22. Kransdorf MJ, Jelinek JS, Moser RP, et al. Soft tissue masses: diagnosis using MR imaging. AJR Am J Roentgenol 1989; 153:541–547.
23. Weekes RG, Berquist TH, McLeod RA, Zimmer WD. Magnetic resonance imaging of soft tissue tumors: comparison with computed tomography. Magn Reson Imaging 1985; 3:345–352.
24. Berquist TH, Ehman RL, King BF, Hodgman CG, Ilstrup DM. Value of MRI in differentiating benign from malignant soft tissue masses: study of 95 lesions. AJR Am J Roentgenol. 1990; 155:1251–1255.
25. Glass-Royal MC, Nelson MC, Albert F, Lack EE, Bogumill GP. Case report 557: solitary intramuscular myxoma in a patient with polyostotic fibrous dysplasia. Skeletal Radiol 1989; 18:392–398.
26. Gober GA, Nicholas RW. Case Report 800: skeletal fibrous dysplasia associated with intramuscular myxoma (Mazabraud's syndrome). Skeletal Radiol 1993; 6:452–455.
27. Lassance Cabral CE, Guedes P, Fonseca T, Rezende JF, Cruz LC, Smith J. Polyostotic fibrous dysplasia associated with intramuscular myxomas: Mazabraud's syndrome. Skeletal Radiol 1998; 27:278–282.
28. Abdelwahab IF, Kenan S, Hermann G, Klein MJ, Lewis MM. Intramuscular myxoma of the left forearm. Bull Hosp Jt Dis 1993; 53(3):15–17.
29. Kamoun N, Zouari M Siala S, et al. Myxome intra-musculaire. A propos de deux localisations. Rev Chir Orthop 1997; 83:278–282.
30. Suzuki T, Mio A, Suzaki K, et al. An evaluation of MR imaging of soft-tissue masses in extremities. Rinsho Hoshasen 1990; 35: 69–75.
31. Enzinger FM. Intramuscular myxoma: a review and follow-up study of 34 cases. Am J Clin Pathol 1965; 43:104–113.
32. Walker RE, Schwartz RK, Gale DR. Musculoskeletal case of the day. Mazabraud's syndrome (intramuscular myxoma associated with fibrous dysplasia of bone). AJR Am J Roentgenol 1999; 173:797, 800–802.

33. Struk DW, Munk PL, Lee MJ. Musculoskeletal case 8: Mazabraud's syndrome—intramuscular myxoma associated with fibrous dysplasia. Can J Surg 2000; 43:62–63.
34. Guppy KH, Wagner F, Tawk R, Gallagher L. Intramuscular myxoma causing lumbar radiculopathy. Case report and review of the literature. Neurosurgery 2001; 95(2 Suppl):260–263.
35. Delabrousse E, Couvreur M, Bartholomot B, Lucas X, Kastler B. Mazabraud syndrome: a case diagnosed with MRI. J Radiol 2001; 82:165–167.
36. Iwasko N, Steinbach LS, Disler D, et al. Imaging findings in Mazabraud's syndrome: seven new cases. Skeletal Radiol 2002; 31:81–87.
37. Bancroft LW, Kransdorf MJ, Menke DM, O'Connor MI, Foster WC. Intramuscular myxoma. Characteristic MR imaging features. AJR Am J Roentgenol 2002; 178:1255–1259.
38. Murphey MD, McRae GA, Fanburg-Smith JC, Temple T, Levine AM, Aboulafia AJ. Imaging of soft tissue myxoma with emphasis on CT and MR and comparison of radiological and pathologic findings. Radiology 2002; 225:215–224.
39. Silver WP, Harrelson JM, Scully SP. Intramuscular myxoma: a clinicopathological study of 17 patients. Clin Orthop 2002; 403:191–197.
40. Ly JQ, Bau JL, Beall DP. Forearm intramuscular myxoma. AJR Am J Roentgenol 2003; 181:960.
41. Nishimoto K, Kusuzaki K, Matsumine A, et al. Surrounding muscle edema detected by MRI is valuable for diagnosis of intramuscular myxoma. Oncol Rep 2004;11:143–148.
42. Nielsen GP, O'Conell JX, Rosenberg AE. Intramuscular myxoma: a clinicopathological study of 51 cases with emphasis on hypercellular and hypervascular variants. Am J Surg Pathol 1998; 22: 1222–1227.
43. Enzinger FM, Weiss SW. Benign soft tissue tumors of uncertain type. In: Enzinger FM, Weiss SW. Soft tissue tumors, 3rd edn. St Louis: Mosby, 1994:1045–1051.
44. Henschen F. Fall von Ostitis fibrosa mit multiplen Tumoren in der umgebeden Muskulature. Verh Dtsch Ges Pathol 1926; 21:93.
45. Mazabraud A, Semat P, Rose R. A propos de l'association de fibromixomes des tissus mous à la dysplasie fibreuse des os. Presse Med 1967; 75:2223–2228.
46. Logel RJ. Recurrent intramuscular myxoma associated with Albright's syndrome J Bone Joint Surg Am 1976; 58:565–568.
47. Lever EG, Pettingale RW. Albright's syndrome associated with a soft tissue myxoma and hypophosphatemic osteomalacia: report of a case and a review of the literature. J Bone Joint Surg Br 1983; 65:621–626.
48. Witkin GB, Guildford WB, Siegal GP. Osteogenic sarcoma and soft tissue myxoma in a patient with fibrous dysplasia and hemoglobins J Baltimore and S. Clin Orthop 1986; 204:245–252.
49. Wirth A, Leavitt D, Enzinger FM. Multiple intramuscular myxomas: another extraskeletal manifestation of fibrous dysplasia. Cancer 1971; 27:1167–1173.
50. Berkhoff WBC, ter Bruggen Hugenholtz RI, Ingenhoes R. A patient with multiple intramuscular myxomas with fibrous dysplasia. Ned Tijdschr Geneskd 1981; 125:1460–1462.
51. Sedmark DD, Hart WR, Bellhobek GH, Marks KE. Massive intramuscular myxoma associated with fibrous dysplasia of bone. Cleve Clin Q 1983; 50:469–472.
52. Segev Z, Reiner S. Intramuscular myxoma associated with fibrous dysplasia. Harefuah 1985; 16:493–494.
53. Biagini R, Ruggieri P, Boriani S, Picci P. The Mazabraud's syndrome: case report and review of the literature. Ital J Orthop Traumatol 1987; 1:105–111.
54. Sundaram M, McDonald DJ, Merenda G. Intramuscular myxoma: a rare but important association with fibrous dysplasia of bone. AJR Am J Roentgenol 1989; 153:107–108.
55. Gianoutsos MP, Thompson JF, Marsden FW. Mazabraud's syndrome: intramuscular myxoma associated with fibrous dysplasia of bone. Aust N Z J Surg 1990; 10:825–828.
56. Fujii K, Inove M, Araki Y, Ishida O. Multiple intramuscular myxomas associated with polyostotic fibrous dysplasia. Eur J Radiol 1996; 2:152–154.
57. Limouzy F, Durroux R, Chiron P, Tricoire JL, Puget J, Utheza G. Fibrous dysplasia associated with intramuscular myxoma. Rev Chir Orthop Repartrice Appar Mot 1996; 82:336–339.
58. Prayson MA, Leeson MC. Soft-tissue myxomas and fibrous dysplasia of bone. Clin Orthop 1993; 291:222–228.
59. Rodenberg J, Jensen OM, Keller J, Nielsen OS, Bunger C, Jurik AG. Fibrous dysplasia of the spine, costal and hemipelvis with sarcomatous transformation. Skeletal Radiol 1996; 25:665–684.
60. Lopez-Ben R, Pitt MJ, Jaffe KA, Siegal GP. Osteosarcoma in a patient with McCune-Albright syndrome and Mazabraud's syndrome. Skeletal Radiol 1999; 28:522–526.
61. Parisi B, Cavallera A, Cerrone M, Pecoraro C, Del Viscovo L. Mazabraud's síndrome. A case report. Radiol Med (Torino). 1999; 98:405–407.
62. Faivre L, Nivelon-Chevalier A, Kottler ML, et al. Mazabraud syndrome in two patients: clinical overlap with McCune-Albright syndrome. Am J Med Genet 2001; 99:132–136.
63. Pollandt K, Lohmann CH, Werner M, et al. Clinical pathological aspects of Mazabraud's syndrome. Pathologe 2002; 23:357–360.
64. van Roggen JF, Hogendoorn PCW, Fletcher CDM. Myxoid tumors of soft tissues. Histopathology 1999; 35:291–312.
65. Murphey MD, Smith WS, Smith SE, Kransdorf MJ, Temple HT. From the archives of the AFIP. Imaging of musculoskeletal neurogenic tumors: radiologic-pathologic correlation. Radiographics 1999;19:1253–1280.
66. Murphey MD, Walker EA, Wilson AJ, et al. Imaging of primary chondrosarcoma: radiologic-pathologic correlation. Radiographics 2003; 23:1245–1278.
67. Sundaram M, Baran G, Merenda G, McDonald DJ. Myxoid liposarcomas: magnetic resonance imaging appearances with clinical and histological correlation. Skeletal Radiol 1990; 19:359–362.
68. Jelinek JS, Kransdorf MJ, Schomookler BM, Aboufalia AJ, Malawer MM. Liposarcoma of the extremities: MR and CT findings in the histologic subtypes. Radiology 1993; 186:455–459.
69. Arkun R, Memis A, Akalin T, Ustun EE, Sabah D, Kandiloglu G. Liposarcoma of soft tissue: MRI findings with pathologic correlation. Skeletal Radiol 1997; 26:167–172.
70. London J, Kim E, Wallace S, Shirkoda A, Coan J, Evans H. MR imaging of liposarcomas: correlation of MR features and histology. J Comput Assist Tomogr 1989; 13:832–835.
71. Marques MC, Garcia H. Lipomatous tumors. In: Soft tissue tumors imaging. Berlin Heidelberg New York: Springer, 1997:191–208.
72. Miller TT, Hermann G, Abdelwahab IF, Klein MJ, Kenan S, Lewis MM. MRI of malignant fibrous histiocytoma of soft tissue: analysis of 13 cases with pathologic correlation. Skeletal Radiol 1994; 23:271–275.
73. Murphey MD, Gross TM, Rosenthal HG. Musculoskeletal malignant fibrous histiocytoma: radiopathological correlation. Radiographics 1994; 14:807–826.